2017 IEEE/RSJ International Conference on Intelligent Robots and Systems (IROS)
September 24–28, 2017, Vancouver, BC, Canada

Force Sensing in Continuum Manipulators using Fiber Bragg Grating Sensors

Fouzia Khan, Roy J. Roesthuis and Sarthak Misra

***Abstract*— The presence of force feedback in medical instruments has been proven to reduce tissue damage. In order to provide force feedback, information about the interaction forces between the instrument and the environment must be known. Direct measurement of these forces by commercial sensors is not feasible due to space limitations. Thus, in this study we propose to estimate the interaction forces using strain measurements from Fiber Bragg Grating (FBG) sensors. These measurements can also be used for shape sensing and as a result both force and shape can be sensed simultaneously. For force sensing two models are proposed and compared. The first is based on a Rigid Link approximation, while the second uses the Cosserat rod theory. The models are validated experimentally using a tendon-driven continuum manipulator that is subjected to forces at the tip. The force estimates from the models are compared to the measurements from a commercial force sensor. Mean absolute errors of 11.2 mN (6.9%) and 15.9 mN (8.3%) are observed for the Rigid Link model and Cosserat model, respectively.**

I. Introduction

Many of the instruments currently used in medical procedures have a mechanical design similar to continuum manipulators [1]. Examples of such instruments are colonoscopes, endoscopes and other flexible catheters for procedures such as cardiac surgery and bronchoscopy. Some continuum manipulators have been developed specifically for medical applications. These include multi-backbone system for throat surgery, concentric tube active cannula for cardiac surgery and steerable probe for neurosurgery [2]–[4]. These manipulators can be easily miniaturized and they provide a larger workspace compared to rigid tools, thus they are ideal for minimally invasive procedures [1]. However, the disadvantage of using such manipulators is the loss of force information at the tip. Having accurate knowledge about the interaction forces between the manipulator and tissue is important for the outcome of the procedure [5]. It can be used to provide surgeons with force feedback, thereby enabling more precise manipulation of the tissue. Sensing forces accurately at the manipulator tip is challenging because the available space does not allow integration of commercially-available force sensors. Considering further miniaturization of manipulator size in the future, there is a need for alternative methods for sensing interaction forces on manipulators for medical applications.

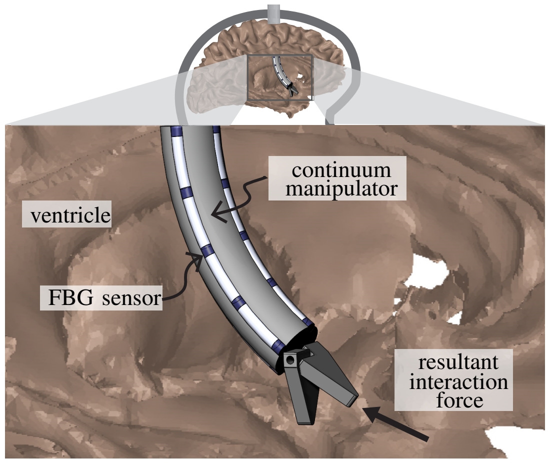

Fig. 1. Minimally invasive neurosurgery is an example of a procedure that can benefit from instruments like continuum manipulators that provide a larger workspace compared to rigid manipulators. Fiber Bragg Grating (FBG) sensors can be used to acquire information about the interaction forces and the shape of the instrument.

A number of studies have proposed methods to identify the interaction forces on manipulators without measuring them directly. For example, Xu and Simaan presented a method that used the deflected shape of the manipulator shaft to estimate the force at the tip [6], [7]. Rucker and Webster estimated the tip force by using pose measurements and a kinematic static model of the continuum manipulator with measurement uncertainty [8]. They described the tip force as a state of the system, and an extended Kalman filter was used to estimate the system states from the noisy end-effector pose measurements. Back *et al*. estimated the tip force using shape of the catheter and the Cosserat rod model [9]. Lastly, Khosnam *et al*. used the curvature of a catheter, determined from camera images, in combination with a kinematic model to estimate the tip contact force [10].

Another approach to force estimation is to sense the strains on the manipulator directly using sensors. The benefit of using an independent sensor for force is that the robustness of the system to sensor failure will improve due to redundancy and in theory direct measurement of strain will lead to more accurate force estimation. A suitable sensor for medical applications is the Fiber Bragg Grating sensor because it is small in size, sterilizable, biocompatible, highly sensitive to strain, and compatible with medical imaging modalities [11]. The FBG sensors can be embedded in instruments

F. Khan and R.J. Roesthuis equally contributed to this work. This research has received funding from the European Union's Horizon 2020 research and innovation programme under Grant Agreement #688279 (EDEN2020) and by the Dutch Technology Foundation STW (H-Haptics Project #12159) which is part of the Netherlands Organization for Scientific Research. All authors are affiliated with the Surgical Robotics Laboratory, Department of Biomechanical Engineering, MIRA - Institute for Biomedical Technology and Technical Medicine, University of Twente, 7522 NB, The Netherlands. F. Khan and S. Misra are also affiliated with the Department of Biomedical Engineering, University of Groningen and University Medical Center Groningen, 9713 GZ, The Netherlands.

978-1-5386-2681-8/17/$31.00 ©2017 IEEE

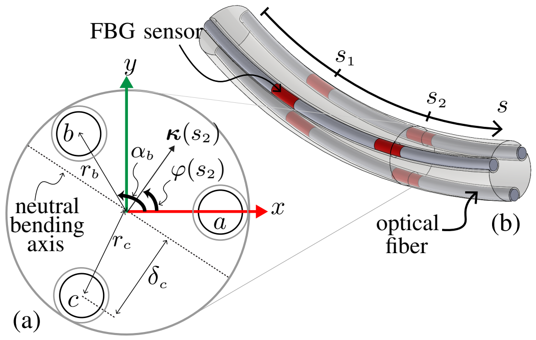

Fig. 2. Shape reconstruction using Fiber Bragg Grating (FBG). (a) The manipulator curvature ($\boldsymbol{\kappa}$) and bending direction (φ) are calculated using strain measurements from a set of three co-located FBG sensors on fibers a, b, and c. Distance from the center of the manipulator to the center of fibers b and c is r_b and r_c, respectively. Angle from x-axis to r_b is α_b and the perpendicular distance between the neutral bending axis and center of fiber c is δ_c. (b) The curvature is calculated from the strain measured at discrete locations (s_k) that have co-located FBG sensors.

for angioplasty, gastric endoluminal surgery or minimally invasive neurosurgery in order to measure interaction forces (Figure 1). These sensors have been used near the tip of medical instruments to measure only axial forces [12]–[14]. They have also been helically wrapped around the shaft of a manipulator in order to determine the wrench at the tip [15]. However, this approach can not be applied to all manipulators because of mechanical constraints, an example is the manipulator in Burrows *et al.*, thus another sensor placement configuration is required [16].

In this paper, the contact forces at the tip of a continuum manipulator are estimated using strain measurements from FBG sensors placed along the arc length. This placement configuration can also be used for shape sensing, thus enabling simultaneous acquisition of force and shape information. Previously, Roesthuis *et al.* demonstrated the feasibility of sensing forces from FBG sensors by presenting the correlation between measurements from FBG sensor and a commercial force sensor [17]. This paper extends that work - force at the tip of a continuum manipulator is estimated using the FBG sensor measurements in conjunction with a model of the manipulator. In this study, two different models, Rigid Link and Cosserat, are applied and forces estimated from each of these models are compared to the ground truth measurement from a force sensor. Both of the models give force estimates based on the shape information that can be derived from the FBG sensor measurements as described in Section II. The Rigid Link model and the Cosserat model are presented in Sections III and IV, respectively. The experimental results and comparison between the two models are presented in Section V. Lastly Section VI concludes the paper and provides directions for future work. Thus, this paper validates force sensing using FBG sensors and presents a comparison of the two models. This combination of work has not been presented in the literature to the best knowledge of the authors.

II. Shape Reconstruction

The FBG sensors have been used for reconstruction of needle shape during insertion into soft-tissue phantoms, and for shape reconstruction of a tendon-driven continuum manipulator in free-space [18], [19]. Strain measurements from at least 3 co-located FBG sensors are required in order to calculate the magnitude ($\| \boldsymbol{\kappa} \|$) and direction ($\varphi$) of the curvature vector at a specific location (s_k, $k \in \mathbb{Z}_+$) along the manipulator shaft (Figure 2). Each FBG sensor measures a strain (ϵ_*), where $* \in (a, b, c)$, that is given by

$$\begin{aligned}\epsilon_*(s_k) &= \| \boldsymbol{\kappa}(s_k) \| \, \delta_*(s_k) + \epsilon_0, \\ &= \| \boldsymbol{\kappa}(s_k) \| \, r_* cos(\varphi(s_k) - \alpha_*) + \epsilon_0, \end{aligned} \quad (1)$$

where δ_* is the distance from the fiber center to the neutral bending axis, r_* is the distance of the fiber center to the center of the manipulator, α_* is the angle of the fiber with respect to x-axis at the manipulator cross-section, $\boldsymbol{\kappa}(s_k) \in \mathbb{R}^2$ is the curvature vector and $\varphi(s_k) \in \mathbb{R}$ is the direction of bending (Figure 2). Each sensor is assumed to have a common offset (ϵ_0) in the measured strain, that can be caused by a change in the environmental temperature or an axial force along the manipulator shaft. The three unknowns (i.e., $\| \boldsymbol{\kappa} \|$, φ and ϵ_0) are solved from the strains measured by the three co-located FBG sensors. The curvature magnitude ($\| \boldsymbol{\kappa}(s_k) \|$) and the bending direction ($\varphi(s_k)$) can be used to define the curvature vector ($\boldsymbol{\kappa}(s_k)$) at each sensor location:

$$\boldsymbol{\kappa}(s_k) = \begin{bmatrix} \kappa_x(s_k) \\ \kappa_y(s_k) \end{bmatrix} = \| \boldsymbol{\kappa}(s_k) \| \begin{bmatrix} cos(\varphi(s_k)) \\ sin(\varphi(s_k)) \end{bmatrix}. \quad (2)$$

Interpolation of the curvature components ($\kappa_x(s_k)$, $\kappa_y(s_k)$) between each of the FBG sensor locations is performed in order to obtain the curvature vector ($\boldsymbol{\kappa}(s)$) at every location along the manipulator shaft (Figure 2). The bending direction ($\varphi(s)$) along the shaft, is equal to the direction of the curvature vector. The curvature and the bending direction defines the orientation, which can be used to evaluate the tangent vector ($\mathbf{t}(s)$) of the curve and $\mathbf{t}(s) = \frac{d\mathbf{r}}{ds}$, where $\mathbf{r}(s) \in \mathbb{R}^3$ is the position vector of the curve. Hence, manipulator shape can be reconstructed by numerical integration of the tangent vector. The curvature and direction of bending information will be required by both the Rigid Link and Cosserat model.

III. Rigid Link Model

In rigid link robots contact forces/torques at the end-effector are estimated using joint forces/torques [20] [21]. The continuum manipulator is modeled as a rigid link robot with revolute joints [22]. The interaction forces at the tip are determined based on the joint torques in the model.

A. Kinematics

The continuous shape of a manipulator is approximated by a serial chain of n rigid links, connected by n revolute joints (Figure 3). This method can be used to describe non-constant curvature bending, that occur in flexible instruments subjected to external loading. Link orientation is described by three consecutive rotations, thus results in the following rotation matrix of the i-th link with respect to the $i-1$ link:

$$\mathbf{R}_i^{i-1} = \mathbf{R}_z(q_{\varphi,i})\mathbf{R}_y(q_{\theta,i})\mathbf{R}_z(-q_{\varphi,i}), \quad (3)$$

where $\mathbf{R}_z \in SO(3)$ and $\mathbf{R}_y \in SO(3)$ are rotation matrices about the z-axis and y-axis of the rotated frame, respectively (Figure 3). The two joint angles that determine the rotations in (3) are related to the direction of bending ($q_{\varphi,i} \in \mathbb{R}$) and the amount of bending ($q_{\theta,i} \in \mathbb{R}$). In order to describe the manipulator elasticity using the Rigid Link model, each joint is assigned a flexural stiffness that is related to the bending stiffness. In the next sub-section, manipulator statics is used to relate manipulator shape to the manipulator tip wrenches which is the result from actuation and from external loading.

B. Statics

In order to calculate manipulator configuration, the joint angles of the Rigid Link model need to be related to the loads that act on the manipulator. In static equilibrium, the loads that act on the manipulator are balanced by the torques generated in the joints. The joint torques are not generated by motors, but are the result of manipulator bending. The joints are elastic, such that a joint torque (τ_i) at the i-th joint is given by the following relation:

$$\tau_i = K_{\theta,i} q_{\theta,i}, \tag{4}$$

where, $K_{\theta,i}$ is the flexural stiffness, $q_{\theta,i}$ is the amount of bending (Section II), and $\tau_i \in \mathbb{R}$ is the magnitude of the bending moment at the location of the joint. The bending moment $\left(\mathbf{m}(s_i) \in \mathbb{R}^3\right)$ at the i-th joint is the sum of the contribution of an actuation moment and an external force (Figure 3):

$$\mathbf{m}(s_i) = \mathbf{m}_{ac} + \mathbf{r}_F(s_i) \times \mathbf{F}_{ext}. \tag{5}$$

where, $\mathbf{m}_{ac} \in \mathbb{R}^3$ is the actuation moment, $\mathbf{F}_{ext} \in \mathbb{R}^3$ is the external force and $\mathbf{r}_F(s_i) \in \mathbb{R}^3$ is the vector from the external force contact point to joint i. For a continuum manipulator with n rigid links connected by n joints, the joint torque vector ($\boldsymbol{\tau} \in \mathbb{R}^n$) can be written as

$$\boldsymbol{\tau} = \boldsymbol{\tau}_{ac} + \boldsymbol{\tau}_{ext}, \tag{6}$$

where $\boldsymbol{\tau}_{ac} \in \mathbb{R}^n$ and $\boldsymbol{\tau}_{ext} \in \mathbb{R}^n$ are the joint torques due to (internal) actuation and (unknown) external forces, respectively. We assume that actuation generates a pure moment at the end of the manipulator (Figure 3). The joint torques due to the actuation moment ($\mathbf{m}_{ac} \in \mathbb{R}^3$) can be calculated using

$$\boldsymbol{\tau}_{ac} = \mathbf{J}_m^T \begin{bmatrix} \mathbf{0}_3 \\ \mathbf{m}_{ac} \end{bmatrix} = \mathbf{J}_m^T \mathbf{w}_{ac}, \tag{7}$$

where $\mathbf{J}_m \in \mathbb{R}^{6\times n}$ is the manipulator Jacobian, $\mathbf{0}_3 = [0\ 0\ 0]^T$, and $\mathbf{w}_{ac} \in \mathbb{R}^6$ denotes the actuation wrench. The contribution to the joint torque vector in (6) is given by

$$\boldsymbol{\tau}_{ext} = \mathbf{J}_{cp}^T \begin{bmatrix} \mathbf{F}_{ext} \\ \mathbf{0}_3 \end{bmatrix} = \mathbf{J}_{cp}^T \mathbf{w}_{ext}, \tag{8}$$

where $\mathbf{J}_{cp} \in \mathbb{R}^{6\times n}$ is the contact point Jacobian. The above formulation will be used in combination with shape information ($q_{\varphi,i}$ and $q_{\theta,i}$) derived from FBG sensor measurements. The next section presents the rigid link model fitting based on the shape information.

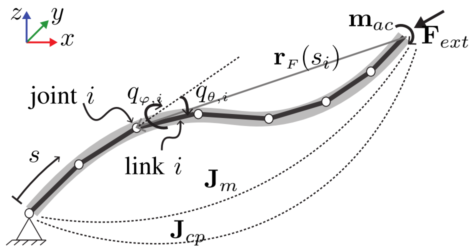

Fig. 3. Rigid Link Model: The continuum manipulator is illustrated as bold gray curve and its shape is approximated by a serial chain of seven rigid links that are connected by revolute joints. This description enables calculation of manipulator shape under a combination of internal actuation moments ($\mathbf{m}_{ac}$) and external force ($\mathbf{F}_{ext}$). $\mathbf{J}_m$ and $\mathbf{J}_{cp}$ are the manipulator and contact point Jacobians, respectively. The amount of bending at joint i is given by $q_{\theta,i}$ and the direction of bending is given by $q_{\varphi,i}$. The vector from the contact point to joint i is $\mathbf{r}_F(s_i)$.

C. Rigid Link Model Fitting

The model consists of n joints and n rigid links, each joint has two degrees of freedom, one related to the bending and the other related to the direction of bending. The joint angles can be determined from the curvature vector $\left(\boldsymbol{\kappa}(s) \in \mathbb{R}^2\right)$ and bending direction ($\varphi(s) \in \mathbb{R}$), which are calculated from FBG sensors (Section II). The joint angles that define the configuration of the Rigid Link model can be related to the curvature vector. Integrating the curvature magnitude gives the slope ($\theta(s) \in \mathbb{R}$) along the shaft:

$$\theta(s) = \int_0^s \|\boldsymbol{\kappa}(s)\| \mathrm{d}s. \tag{9}$$

The joint angle related to manipulator bending can be calculated from manipulator slope as

$$q_{\theta,i} = \frac{1}{2}\Delta\theta_{i-1} + \frac{1}{2}\Delta\theta_i, \tag{10}$$

where $\Delta\theta_i$ is the change in manipulator slope between two consecutive joints:

$$\Delta\theta_i = \theta(s_{i+1}) - \theta(s_i). \tag{11}$$

The joint angle related to the bending direction equals the curvature direction at the location of the i^{th} joint ($q_{\varphi,i} = \varphi(s_i)$). Manipulator configuration is now fully defined given the curvature vector from the FBG sensor measurements. This allows the derivation of the manipulator Jacobian, which is used in the next section to estimate the unknown external forces.

D. Contact Force Estimation

The joint torque due to the unknown external load is given by $\boldsymbol{\tau}_{ext} = \boldsymbol{\tau} - \boldsymbol{\tau}_{ac}$, where $\boldsymbol{\tau}$ is determined using (4) and $\boldsymbol{\tau}_{ac}$ is from (7). Thus, combining (4) and (7)

$$\boldsymbol{\tau}_{ext} = \begin{bmatrix} \tau_1 \\ \vdots \\ \tau_n \end{bmatrix} = \begin{bmatrix} K_{\theta,1}q_{\theta,1} - \tau_{ac,1} \\ \vdots \\ K_{\theta,n}q_{\theta,n} - \tau_{ac,n} \end{bmatrix}. \tag{12}$$

The contact points are assumed to be known for all (unknown) external loads, such that the Jacobian ($\mathbf{J}_{cp}$) for the contact point can be determined using the forward kinematics of the Rigid Link model. In the case of a single external load ($\mathbf{F}_{ext}$) at the manipulator tip, the contribution to a joint torque vector from the load is given by

$$\boldsymbol{\tau}_{ext} = \mathbf{J}_{cp}^T \begin{bmatrix} \mathbf{F}_{ext} \\ \mathbf{0}_3 \end{bmatrix}, \tag{13}$$

where, $\mathbf{J}_{cp} \in \mathbb{R}^{6\times n}$ and $\mathbf{F}_{ext} \in \mathbb{R}^3$. For multiple external loads $\mathbf{J}_{cp} \in \mathbb{R}^{6m\times n}$, where m is the number of external loads. Since the manipulator Jacobian is often non-square, the external force is estimated using the pseudoinverse of the Jacobian

$$\begin{bmatrix} \mathbf{F}_{ext} \\ \mathbf{0}_3 \end{bmatrix} = (\mathbf{J}_{cp}^T)^{\dagger} \boldsymbol{\tau}_{ext}, \tag{14}$$

where $(.)^{\dagger}$ denotes the Moore-Penrose pseudoinverse, and $\boldsymbol{\tau}_{ext}$ is calculated from (12). Thus, the external force ($\mathbf{F}_{ext}$) is estimated using the Rigid Link model. The next section presents the Cosserat model that can also be utilized to estimate the external force.

IV. Cosserat Model

The Cosserat rod theory presents an geometrically exact model for a flexible rod, this is the motivation for the Cosserat model. The model presented in the paper is applicable to manipulators that have small cross section area compared to their length and are not subjected to torsion or axial forces. The force at the tip of the continuum manipulator can be estimated based on the shape information calculated from the strain measurements of the FBG sensors.

A. Kinematics

The manipulator kinematics is based on a continuous transformation that is a function of the arc length [23]. In general, the transformation is dependent on the strains and shear stress acting on the manipulator, however given the assumption that the manipulator is not subjected to torsion and axial forces, the kinematics can be simplified such that the position $\left(\mathbf{r}(s) \in \mathbb{R}^3\right)$ as a function of the arc length $(s \in \mathbb{R})$ can be determined by solving the following:

$$\mathbf{r}'(s) = \mathbf{R}(s)\mathbf{e}_3, \tag{15}$$

$$\mathbf{R}'(s) = \mathbf{R}(s)\widehat{\mathbf{u}}(s), \tag{16}$$

where $(')$ is the derivative with respect to s, $\mathbf{R}(s) \in SO(3)$ is the rotation matrix and it represents the change in curvature with respect to the arc length, $\mathbf{e}_3 = [0\ 0\ 1]^T$ and $\widehat{\mathbf{u}}(s) \in so(3)$ represents a skew symmetric matrix based on the components of the curvature vector $\left(\mathbf{u}(s) \in \mathbb{R}^3\right)$ that is in local coordinates. $\mathbf{u}(s) = [\kappa_x(s)\ \ \kappa_y(s)\ \ 0]^T$, the last component is zero due to the assumption of no torsion. Frenet-Serret frames are used for the local coordinates; the z_l-axis is tangent to the center curve of the manipulator, the x_l-axis is aligned with the inner normal and the y_l-axis is aligned with the binormal vector (Figure 4).

B. Contact force estimation

The applied force at the tip of the manipulator is calculated using the constitutive relation and equations for equilibrium. The linear constitutive relation is as follows:

$$\mathbf{m}(s) = \mathbf{R}(s)\mathbf{K}(s)\boldsymbol{\Delta}\mathbf{u}(s), \tag{17}$$

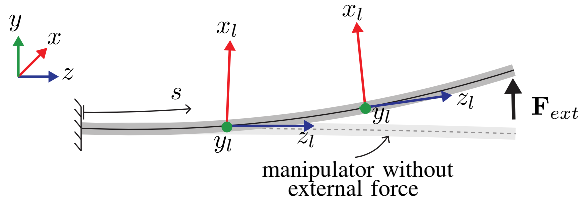

Fig. 4. Cosserat Model: Continuous Frenet-Serret frames are assigned along the centerline curve of the manipulator. The global axis is at the base and the local axis is along the arc length of the manipulator.

where $\boldsymbol{\Delta}\mathbf{u}(s) = \mathbf{u}^*(s) - \mathbf{u}(s)$, $\mathbf{u}^*(s) \in \mathbb{R}^3$ is the curvature vector when no external force is applied and and $\mathbf{u}(s) \in \mathbb{R}^3$ is the curvature vector after the external force is applied on the manipulator, both are in local coordinates. $\mathbf{K}(s) \in \mathbb{R}^{3\times 3}$ is the stiffness matrix. The equations for equilibrium are:

$$\mathbf{n}(s) = \int_s^L \mathbf{f}(\sigma)\mathrm{d}\sigma, \tag{18}$$

$$\mathbf{m}(s) = \int_s^L [\mathbf{r}(\sigma)) \times \mathbf{f}(\sigma)]\mathrm{d}\sigma - \mathbf{r}(s) \times \mathbf{n}(s), \tag{19}$$

where $\mathbf{f}(\sigma) \in \mathbb{R}^3$ is the external force at the tip of the manipulator and $\sigma \in \mathbb{R}$ is a dummy integral variable. The force is modeled as a product of the unknown force $\mathbf{F}_{ext} \in \mathbb{R}^3$ and a shifted Dirac delta function, $\mathbf{f}(\sigma) = \mathbf{F}_{ext}\,\delta(\sigma - L)$, where L is the arc length at which the force is applied. Substituting (17) and (18) into (19) leads to the estimate of the external force $\mathbf{F}_{ext}$ that is given below:

$$\mathbf{F}_{ext} = (\widehat{\boldsymbol{\Delta}\mathbf{r}}(s))^{\dagger}\mathbf{R}(s)\mathbf{K}(s)\boldsymbol{\Delta}\mathbf{u}(s), \tag{20}$$

where $(.)^{\dagger}$ is the Moore-Penrose pseudoinverse and

$$\boldsymbol{\Delta}\mathbf{r}(s) = \mathbf{r}(L) - \mathbf{r}(s), \tag{21}$$

$\widehat{\boldsymbol{\Delta}\mathbf{r}}(s) \in so(3)$ is a skew symmetric matrix based on the vector $\boldsymbol{\Delta}\mathbf{r}(s) \in \mathbb{R}^3$ from (21). The rotation matrix $\mathbf{R}(s)$ in (20) is calculated from (16). Thus, (20) gives the external force based on any point on the arc length and the evaluated parameters on the right hand side of the equation.

V. Experiments And Results

This section presents the experiments used to validate the Rigid Link and Cosserat model, the experimental setup, the calibration procedures and results.

A. Experimental Setup

The experimental setup consists of a continuum manipulator that is actuated by four tendons (DSM Dyneema B.V., Geleen, The Netherlands), shown in Figure 5(a). The backbone (Figure 5(b)) of the manipulator is made from a flexible Polyether ether ketone (PEEK) and it has grooves in which three optical fibers of diameter 250 μm are glued. Each fiber has 8 FBG sensors and the fibers are positioned such that corresponding FBG sensors are co-located (Figure 2). Thus, the backbone has 8 sets of co-located FBG sensors as shown in Figure 5(b). The setup has a linear stage to move the continuum manipulator along the global z-axis, a Deminsys Python FBG interrogator (Technobis group, Alkmaar, The Netherlands) and a Nano-43 6-DOF force/torque sensor (ATI

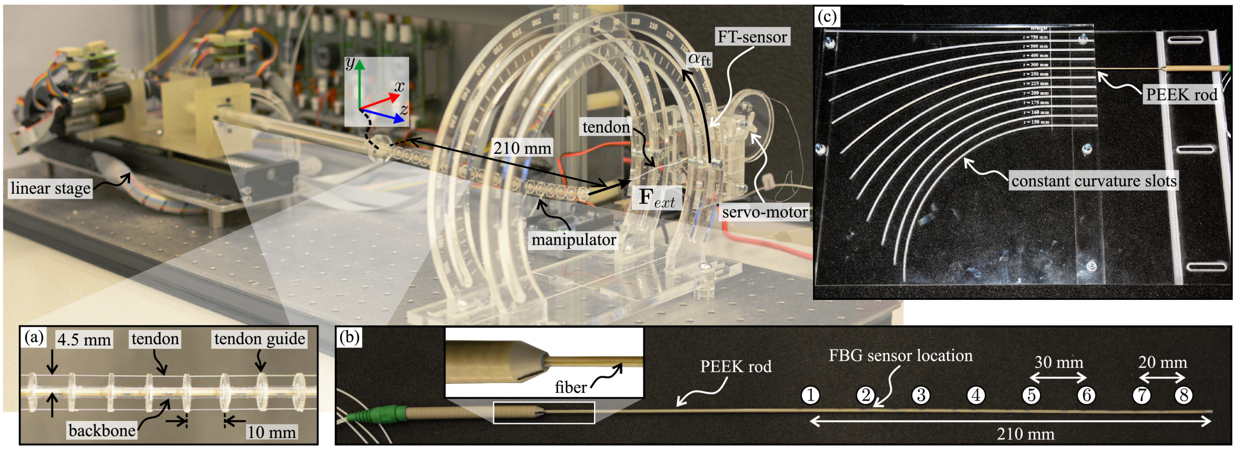

Fig. 5. The tendon-driven manipulator in the experiment setup is 210 mm long and is embedded with Fiber Bragg Grating (FBG) sensors. External tip force ($\mathbf{F}_{ext}$) is applied using a tether that is connected to an ATI Nano-43 force-torque (FT) sensor, which measures the external tip force. (a) Tendon guides (diameter 10 mm) are glued at a spacing of 10 mm along the backbone made from silicon tubing. Four tendons are routed through 20 tendon guides, and are attached to the manipulator tip. (b) The tendon-driven manipulator has a Polyether ether ketone (PEEK) rod embedded in it. Three fibers are glued into grooves along the length of the rod. Each fiber has eight FBG sensors, labeled ①-⑧. (c) Calibration of the FBG sensors is performed by placing the PEEK rod in different circular slots of known curvatures.

Industrial Automation, Apex, USA). The actuation motors for the manipulator are Maxon EC-max 283840 (Maxon motor AG, Sachseln, Switzerland) and they are driven by Elmo controllers (Elmo Motion Control Ltd., Petach-Tikva, Israel). Controller Area Network (CAN) is used to provide communication with the motor drivers and Ethernet is used for communication with the interrogator and the force sensor.

B. Calibration

In order to accurately calculate curvature from the measured strains, the exact distance of the fiber from the center of the manipulator at the location of the sensor needs to be known. The shape sensing rod is placed in several constant curvature slots, which are laser cut in an acrylic plate (Figure 5(c)). Each fiber is separately calibrated by aligning the fiber with the bending direction of the rod. Using the curvature of the slot and the measured strain, the distance (r_a, r_b and r_c, (Figure 2)) between the fiber and the center of the rod at each sensor location is calculated. The average value for all slots is calculated, and is used as the calibrated distance (Table I). These values are used to calculate the curvature vectors from the strain measurements, as described in Section II.

The flexural stiffness ($K_{\theta,i}$ in (4)) required by the Rigid Link model and the stiffness matrix ($\mathbf{K}(s)$ in (17)), required by the Cosserat rod model are determined experimentally due to unavailability of accurate material properties. Data from 14 experiments in conjunction with *lsqlin* (MATLAB R2015b, The MathWorks Inc., Natick, MA) is utilized to solve for the stiffness parameters. The remaining experiments were used to validate the models.

TABLE I

MEAN (STANDARD DEVIATION IN BRACKETS) DISTANCES (IN μM) OF FBG SENSORS (r_a, r_b AND r_c) AFTER CALIBRATION

sensor #	1	2	3	4	5	6	7	8
r_a	672 (20)	743 (9)	767 (13)	802 (19)	774 (11)	748 (9)	696 (14)	412 (62)
r_b	611 (14)	695 (8)	697 (10)	704 (14)	701 (17)	681 (4)	603 (13)	289 (16)
r_c	611 (31)	672 (21)	695 (29)	722 (18)	729 (35)	683 (13)	663 (23)	413 (53)

C. Experiments

The Rigid Link and the Cosserat models are validated using a tendon-driven continuum manipulator (Figure 5(a)). An external force ($\mathbf{F}_{ext}$) is applied to the tip of the manipulator from three directions (α_{ft}) which are 0°, 90° and 180° with respect to the global x-axis (Figure 5). The manipulator tip is tethered to the force sensor and the sensor is manually placed such that the tether is in-line with one of the three directions. Once the sensor is placed, the tension in the tether is increased, which results in an external force at the manipulator tip in the α_{ft} direction. The experiment is repeated 10 times for each direction and the measurements from the FBG sensors and the force sensor are collected. Inputs to the two models are the measurements from the FBG sensors and the output is the tip force estimate. In the next sub-section, the force sensor measurement is compared to the force estimate from both models.

D. Results

The magnitude of the force from the sensor and the models are compared for all experiments. The plot of the force measured and the force estimated from a representative experiment is presented in Figure 6. It shows that both models can track the change in applied force. The mean error ($\overline{\mathrm{e}}$) and the mean relative error ($\overline{\mathrm{re}}$) as defined in (22) and (23) are reported in Table II.

$$\mathrm{e}(t) = \mid (\parallel \mathbf{F}_{sen}(t) \parallel - \parallel \mathbf{F}_{mdl}(t) \parallel) \mid, \tag{22}$$

$$\mathrm{re}(t) = \frac{\mathrm{e}(t)}{\parallel \mathbf{F}_{sen}(t) \parallel} \; s.t \parallel \mathbf{F}_{sen}(t) \parallel > 0, \tag{23}$$

where $t \in \mathbb{R}$ represents time, $\mathbf{F}_{sen}(t) \in \mathbb{R}^3$ is the force measurement from the sensor and $\mathbf{F}_{mdl}(t) \in \mathbb{R}^3$ is the force estimate from the models.

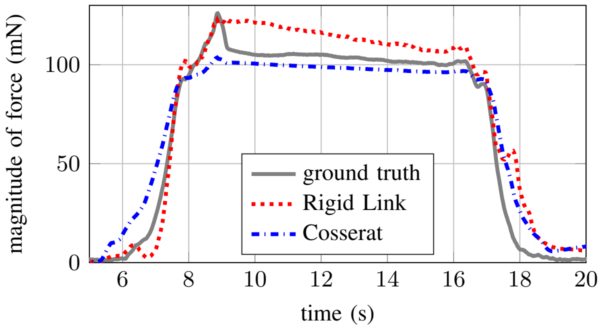

Fig. 6. Representative plot from an experiment where the tip force ($\mathbf{F}_{ext}$) is applied in the $\alpha_{ft} = 180°$ direction. The output from the models is compared to the force sensor measurement (ground truth).

The errors are reported for all the experiments and for experiments with the same direction of applied force (α_{ft}). This approach aids in observing the behavior of the models in relation to the direction of the applied force. The results show that both models have similar performances and that force in the x-z plane are better estimated. On average, the Rigid Link model has a smaller error compared to the Cosserat model and it is computationally less complex.

TABLE II

MODEL COMPARISON: MEAN ERROR ($\overline{\text{e}}$) WITH STANDARD DEVIATION IN BRACKETS AND MEAN RELATIVE ERROR ($\overline{\text{re}}$) FOR EXPERIMENTS WITH APPLIED FORCE IN α_{ft} DIRECTION AND FOR ALL EXPERIMENTS

α_{ft}		0°	90°	180°	All
Rigid Link	$\overline{\text{e}}$ (mN)	5.6 (6.0)	19.7 (20.8)	6.5 (7.1)	11.2 (15.3)
	$\overline{\text{re}}$ (%)	6.9	6.1	6.9	6.9
Cosserat	$\overline{\text{e}}$ (mN)	8.2 (9.6)	29.4 (31.9)	7.6 (7.1)	15.9 (23.1)
	$\overline{\text{re}}$ (%)	6.2	11	7.5	8.3

VI. CONCLUSIONS

This paper provides a framework for the FBG sensors that can be utilized for simultaneous shape and force sensing in continuum manipulators. In addition, two models for force sensing are presented and validated on a tendon driven continuum manipulator. The results show that the Rigid Link and Cosserat models can estimate the applied tip forces with an error of 11.2 mN (6.9%) and 15.9 mN (8.3%), respectively. For future work, the wrenches along the shaft of the manipulator and the axial force will be included in the models. The estimated forces could be used for closed loop force control coupled with other clinical imaging modalities for accurate manipulation.

REFERENCES

[1] R. J. Webster and B. A. Jones, "Design and Kinematic Modeling of Constant Curvature Continuum Robots: A Review," *The International Journal of Robotics Research*, vol. 29, no. 13, pp. 1661–1683, 2010.

[2] N. Simaan, K. Xu, A. Kapoor, W. Wei, P. Kazanzides, P. Flint, and R. Taylor, "Design and Integration of a Telerobotic System for Minimally Invasive Surgery of the Throat." *The International Journal of Robotics Research*, vol. 28, no. 9, pp. 1134–1153, 2009.

[3] A. H. Gosline, N. V. Vasilyev, E. J. Butler, C. Folk, A. Cohen, R. Chen, N. Lang, P. J. del Nido, and P. E. Dupont, "Percutaneous intracardiac beating-heart surgery using metal MEMS tissue approximation tools," *The International Journal of Robotics Research*, vol. 31, no. 9, pp. 1081–1093, 2012.

[4] S. Bano, S. Y. Ko, and F. Rodriguez, "Smooth Path Planning for a Biologically-Inspired Neurosurgical Probe," in *Proceedings of the Annual International Conference of the IEEE Engineering in Medicine and Biology Society*, pp.920–923, San Diego, USA, 2012.

[5] C. R. Wagner, N. Stylopoulos, and R. D. Howe, "The role of force feedback in surgery: Analysis of blunt dissection," in *Proceedings of the Tenth Symposium on Haptic Interfaces for Virtual Environment and Teleoperator Systems*, pp.68–74, Orlando, USA, Mar 2002.

[6] K. Xu and N. Simaan, "An Investigation of the Intrinsic Force Sensing Capabilities of Continuum Robots," *IEEE Transactions on Robotics*, vol. 24, no. 3, pp. 576–587, 2008.

[7] K. Xu and N. Simaan, "Intrinsic Wrench Estimation and its Performance Index for Multisegment Continuum Robots," *IEEE Transactions on Robotics*, vol. 26, no. 3, pp. 555–561, 2010.

[8] D. C. Rucker and R. J. Webster, "Deflection-based force sensing for continuum robots: A probabilistic approach," in *Proceedings of the IEEE International Conference on Intelligent Robots and Systems*, pp.3764–3769, San Francisco, USA, Sept 2011.

[9] J. Back, T. Manwell, R. Karim, K. Rhode, K. Althoefer, and H. Liu, "Catheter contact force estimation from shape detection using a real-time Cosserat rod model," in *Proceedings of the IEEE International Conference on Intelligent Robots and Systems*, pp.2037–2042, Hamburg, Germany, Sept 2015.

[10] M. Khoshnam, A. C. Skanes, and R. V. Patel, "Modeling and estimation of tip contact force for steerable ablation catheters," *IEEE Transactions on Biomedical Engineering*, vol. 62, no. 5, pp. 1404–1415, 2015.

[11] S. C. Ryu and P. E. Dupont, "FBG-based Shape Sensing Tubes for Continuum Robots," in *Proceedings of the IEEE International Conference on Robotics and Automation*, pp.3531–3537, Hong Kong, China, may 2014.

[12] B. Gonenc and I. Iordachita, "FBG-Based Transverse and Axial Force-Sensing Micro-Forceps for Retinal Microsurgery," in *Proceedings of the IEEE Sensors*, pp.5–7, Orlando, USA, Oct 2016.

[13] S. Elayaperumal, J. H. Bae, D. Christensen, M. R. Cutkosky, B. L. Daniel, R. J. Black, J. M. Costa, F. Faridian, and B. Moslehi, "MR-compatible biopsy needle with enhanced tip force sensing," in *Proceedings of the World Haptics Conference*, pp.109–114, Daejeon, Korea, April 2013.

[14] L. Xu, M. I. Miller, J. Ge, K. R. Nilsson, Z. T. H. Tse, and M. P. Fok, "Temperature-Insensitive Fiber-Optic Contact Force Sensor for Steerable Catheters," *IEEE Sensors*, vol. 16, no. 12, pp. 4771–4775, 2016.

[15] R. Xu, A. Yurkewich, and R. V. Patel, "Curvature , Torsion , and Force Sensing in Continuum Robots Using Helically Wrapped FBG Sensors," *IEEE Robotics and Automation Letters*, vol. 1, no. 2, pp. 1052–1059, 2016.

[16] C. Burrows, R. Secoli, and F. Rodriguez, "Experimental Characterisation of a Biologically Inspired 3D Steering Needle," in *Proceedings of the International Conference on Control, Automation and Systems*, pp.1–6, Gwangju, Korea, Oct 2013.

[17] R. J. Roesthuis and S. Misra, "Steering of Multisegment Continuum Manipulators," *IEEE Transactions on Robotics*, vol. 32, no. 2, pp. 372–382, 2016.

[18] R. J. Roesthuis, S. Janssen, and S. Misra, "On using an array of fiber Bragg grating sensors for closed-loop control of flexible minimally invasive surgical instruments," in *Proceedings of the IEEE/RSJ International Conference on Intelligent Robots and Systems*, pp.2545–2551, Tokyo, Japan, Nov 2013.

[19] R. J. Roesthuis, M. Kemp, J. J. V. D. Dobbelsteen, and S. Misra, "Three-Dimensional Needle Shape Reconstruction Using an Array of Fiber Bragg Grating Sensors," *IEEE/ASME Transactions on Mechatronics*, vol. 19, no. 4, pp. 1115–1126, 2014.

[20] K. S. Eom, I. H. Suh, W. K. Chung, and S. R. Oh, "Disturbance Observer Based Force Control of Robot Manipulator without Force Sensor," in *Proceedings of the IEEE International Conference on Robotics and Automation*, pp.3012–3017, Leuven, Belgium, May 1998.

[21] N. Likar and L. Žlajpah, "External joint torque-based estimation of contact information," *International Journal of Advanced Robotic Systems*, vol. 11, no. 7, pp. 1–11, 2014.

[22] T. Greigarn and M. C. Çavuşoğlu, "Pseudo-Rigid-Body Model and Kinematic Analysis of MRI-Actuated Catheters," in *Proceedings of the IEEE International Conference on Robotics and Automation*, pp.2236–2243, Washington, USA, May 2015.

[23] D. C. Rucker, B. A. Jones, and R. J. Webster, "A geometrically exact model for externally loaded concentric-tube continuum robots," *IEEE Transactions on Robotics*, vol. 26, no. 5, pp. 769–780, 2010.